
This is an electronic reprint of the original article.
This reprint may differ from the original in pagination and typographic detail.

Collins, Steven; Fink, Gerhard

Grain angle determination of silver birch by laser light scattering and tensile fracturing

Published in:
Materials and Structures

DOI:
[10.1617/s11527-022-01995-9](https://doi.org/10.1617/s11527-022-01995-9)

Published: 01/07/2022

Document Version
Publisher's PDF, also known as Version of record

Published under the following license:
CC BY

Please cite the original version:
Collins, S., & Fink, G. (2022). Grain angle determination of silver birch by laser light scattering and tensile fracturing. *Materials and Structures*, 55(6), Article 162. <https://doi.org/10.1617/s11527-022-01995-9>



Grain angle determination of silver birch by laser light scattering and tensile fracturing

Steven Collins · Gerhard Fink

Received: 14 July 2021 / Accepted: 14 June 2022 / Published online: 10 July 2022
© The Author(s) 2022

Abstract Reliable non-destructive methods for grain angle determination are essential for the evaluation of mechanical properties of timber. In the present study, the detection of grain angle by means of laser light scattering patterns is investigated on small-scale specimens and timber boards of silver birch, along with the relationship to fracture angle and tensile strength. Results on small-scale specimens indicate applicability of laser scattering method, as the detected grain angles and the fracture angles show a strong correlation, $r = 0.94$. Three-dimensional grain angles, derived from surface grain angles, show a well defined relationship to strength, which can be described with wood-based failure criteria from literature. Furthermore, the paper presents new findings regarding the detection of flame wood through laser scattering. It was shown that small-scale specimens with flame wood tend to have higher grain angles, higher density, and lower strength, relative to specimens without. Nevertheless, for timber boards, the influence of flame wood on the strength was insignificant.

Keywords Laser scanning · Fibre direction · Fracture angle · Tension strength · Flame wood feature

1 Introduction

Timber is a natural grown material and as such it can be characterized by a large variability of its material properties [1, 2]. Accordingly, viable non-destructive methods for quality evaluation are required for its efficient use as a structural material. Typically, timber boards are graded using either visual or machine grading procedures [3]. For hardwoods, strength grading is less established compared to softwoods; nevertheless, in the European standards, a set of strength classes (D-classes) are defined for hardwoods [4]. However, the range of hardwood species and property profiles is wide and certain species may not be efficiently sorted according to the standard classes and procedures. With the aim of diversifying the resource base for timber construction, knowledge on non-destructive quality evaluation methods and grading procedures for different hardwood species, such as birch, is of interest, and thus, multiple studies have been conducted in this direction, e.g. [5–16].

Silver birch (*Betula pendula* Roth.) is a deciduous tree species widespread across Europe and an abundant broadleaved species of Finland and northern Europe. It is valued for its favourable mechanical properties and as such, the inclusion of birch in timber construction could provide value-added solutions. However, it is not currently well established in the building sector, in part due to the underdeveloped state of grading methods for evaluating the mechanical

S. Collins (✉) · G. Fink
Department of Civil Engineering, Aalto University,
Espoo, Finland
e-mail: steven.collins@aalto.fi



quality of sawn timber [17]. Strength grading of birch timber was, nevertheless, investigated in some previous studies; e.g. [5, 8, 10, 16].

For birch, like other hardwood, grain angle is one of the most important factors influencing the mechanical properties of timber elements, in particular the tensile strength [16, 18, 19, 20]. The grain angle can be separated into (1) global slope of grain, caused by spiral growth or curved and tapered tree stems, and (2) localized slope of grain, caused by knots or other defects.

Determination of the global slope of grain is traditionally done by scratching the surface with a scribe tool and manually measuring the slope relative to the longitudinal direction of the timber element [21]. Modern methods employ non-destructive, automated techniques, that indirectly determine the grain angle by means of surface scanning or by taking advantage of the anisotropic properties of wood [22].

Grain angle determination by means of laser light scattering (for softwood denoted as the tracheid effect) is a surface scanning method that takes advantage of the behaviour of light within the fibres of wood. As light propagates more easily along the fibres compared to across them, the overall result produces scattered light with an elliptical shape. The major axis of the ellipse is indicative of the direction of the fibres. Laser scanning is common in machine grading devices for softwoods. For some hardwoods, including birch, it is still under development. Literature investigating laser scattering on various hardwood species show that the grain direction of hardwoods can be effectively measured, e.g. [23–28], albeit, the laser scattering behaviour can be rather different between species [22, 24, 28], requiring species level optimization.

The laser light scattering technique has been shown applicable for birch [29], in which, grain angles on the wood surface and the out-of-plane dive angles were determined on clear wood and knotted samples. In a more recent study [22], three non-destructive methods for grain angle determination were investigated: electric field strength measurement, microwave scanning, and laser light scattering. For birch, laser light scattering was found to be most effective of the three methods. However, the reference grain angle, obtained from manual splitting, contained sources of error and the implemented ellipse detection algorithm was not optimized for birch. Therefore, the authors suggested that a more reliable reference system and a species

dedicated algorithm would provide more informative results on the efficacy of the method.

A factor in the variation of silver birch properties is the so-called flame wood or flamy-grained wood. It is concerned with discrete or continuous wave-like variations in the grain direction. Often associated with curly-grained or masur birch due to their non-linear growth patterns [17, 30], the strength properties of this type of wood may be lower than clear wood [16, 31]. However, studies on the mechanical properties and behaviour of these wood varieties are generally lacking [32].

The present paper aims to investigate laser scattering and imaging technique for the measurement of grain angle on defect-free wood of small-scale and timber board specimens of silver birch. To evaluate the efficacy of the method, a comparison between laser measurements and the tensile fracture angles of small-scale specimens is examined. To evaluate the potential for strength predictions, the relationship between three-dimensional grain angles, derived from surface laser measurements, and tension strength is examined. The paper also investigates the ability of laser scattering to detect flame wood related grain deviations and the influence of flame wood on strength properties. Furthermore, laser imaging of the timber boards is conducted for primary analysis at the scale of structural timber and serves as an indication for further development directions.

2 Materials and method

2.1 Specimens

Silver birch from southern Finland was used in this study. Birch logs were through-and-through sawn into 60 planks, originating from 30 different trees. From the 60 planks, 70 timber boards were obtained (one or two per plank). The location of each timber board within the stem of the tree was identified, for details see previous studies, [33, 34].

All test specimens of this study were cut out of the 70 timber boards with initial dimensions of $l \times w \times t = 4000 \times 120 \times 35 \text{ mm}^3$. Two groups of specimens were investigated: small-scale specimens and large-scale specimens. From the initial timber boards, a 500 mm long piece was cut away from the end with



fewer knots. The 500 mm piece was thereafter used for the small-scale tests (see paragraph below) and the longer piece (in the following denoted as timber boards) was used for the large-scale tests.

On the 500 mm pieces, areas free of knots and other growth irregularities were identified in order to cut out the small-scale specimens. If the defect free area was large enough, two small-scale specimens (denoted as pairs) were cut, otherwise, one small-scale specimen was cut. In total, the sample consisted of 115 small-scale specimens with 45 pairs.

Dimensions of the small-scale specimens are shown in Fig. 1a. Since the radial and tangential directions were inconsistently oriented in the specimens, a square gauge cross section ($15 \times 15 \text{ mm}^2$) was chosen. A gauge length of 200 mm was chosen in order to guaranty that specimens with a smaller grain angle can fail in shear, here the limit is about four degrees.

2.2 Laser imaging

The laser imaging setup was selected to obtain high quality images with sufficiently bright scattering patterns. Low powered (5 mW) red light laser diodes with a wavelength of 650 nm were used. A digital camera (CMOS sensor 8688×5792 pixels) and a standard 35 mm (focal length) lens was used. Camera

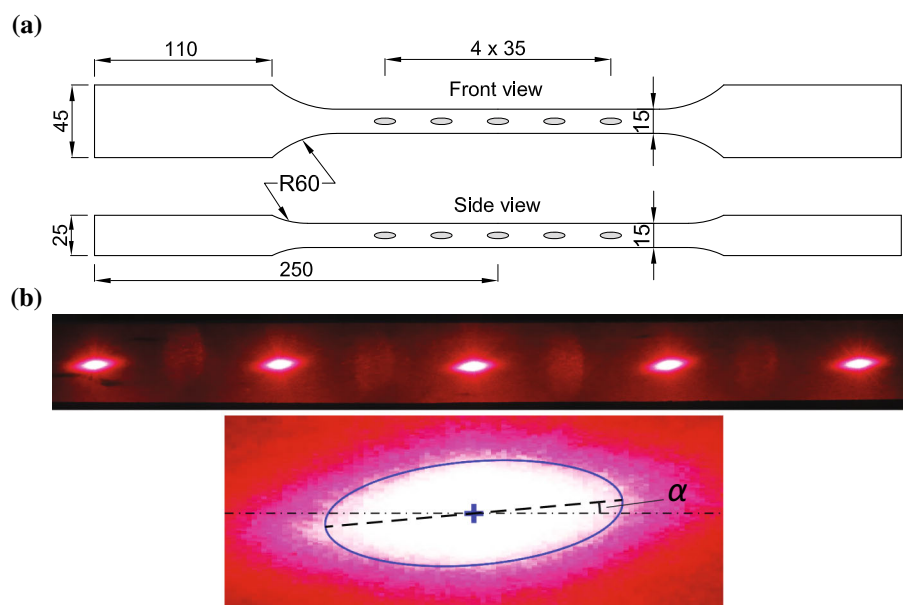
setting were set to: shutter speed, 1/400 s; aperture, $f/3.2$; and ISO 4000.

Five laser points, set along the centre of the measurement area (distance between laser points: 35 mm), were imaged on all four sides of the small-scale specimens (Fig. 1). The average length of the ellipse was 5.8 mm (or 260 pixels). Imaging of the small-scale specimens was conducted prior to tension testing (Sect. 2.5).

For the timber boards, imaging was conducted after tension testing since it was not initially planned to laser image the specimens. However, due to the success of the laser imaging on the small-scale specimens, it was decided to further the investigations and also include the previously tested boards. The fractures of the timber boards suggested that the grain angle over the narrow faces were (predominately) more critical for global grain angle related failures. The particular importance of edgewise slope of grain for visual grading of birch was also mentioned in [8].

To manage the imaging process, each timber board was cut into 350 mm long sections, ten sections per timber board. Five laser points, set along the centre of the measurement area (distance between the laser points: 70 mm) were imaged on both narrow faces. Each section was imaged in sequence. The average length of the imaged ellipses was 7.4 mm (or 210 pixels).

Fig. 1 Laser setup: **a** Schematic illustration of small-scale specimens and laser point measurement locations, dimensions in mm; **b** example of scattered laser points on the surface of a specimen and a magnified view of the detected ellipse, its major axis (dashed line) and the laser angle α



Imaging the timber boards was done primarily to investigate the potential of the laser imaging method on birch timber boards. Adaptation of the method to an automated full-board scanning system is certainly possible.

2.3 Laser angle determination

Digital images of the elliptical scattering patterns are input into a computer algorithm to determine the laser angle. Afterwards, an ellipse is fit to the isolated region. From the ellipse, the length (major and minor axis) and the orientation of the major axis relative to the longitudinal axis of the test piece (denoted as α) was determined, Fig. 1b. These features can be extracted according to the second central moments of the ellipse regions and a principal component analysis (e.g. [35]). To reduce error associated with ill-defined ellipses (i.e. more circular scattering patterns) only ellipses with a minor-to-major axis length ratio ≤ 0.6 were accepted for laser angle determination. In this study, this was the vast majority of the laser points, with 2262/2300 and 6593/7000 for the small-scale specimens and timber boards, respectively.

2.4 Laser angle characterisation

Depending on the specific purpose, different laser angles are required. For comparisons with the surface-wise fracture path or scribing angle, a laser angle representing the surface, α , is needed. In contrast, for comparisons with the tensile strength a three-dimensional laser angle, denoted α_{3D} , is more appropriate. Parameter α_{3D} is determined according to [25, 36] using Eq. 1, where α_i are the laser angles measured on surface i . Surfaces 1 and 3 and surfaces 2 and 4 denote opposite (parallel) sides of the specimen. It is determined only for small-scale specimens.

$$\alpha_{3D} = \cos^{-1} \left(\cos \left(\frac{\alpha_1 + \alpha_3}{2} \right) \times \cos \left(\frac{\alpha_2 + \alpha_4}{2} \right) \right) \quad (1)$$

From the laser angles, different characteristics (mean and median) are calculated as the average or global grain angle, either over the entire specimen or over the entire fracture zone (denoted with superscript: f). It is mentioned that for strength predictions, often the local (maximum) grain deviations are more relevant,

however, due to the low laser point density in this study, some local deviations may not have been measured and are thus not considered.

2.5 Tension tests and density

Tension tests were conducted to reveal the fracture pattern and determine the ultimate tensile strength f_t . All specimens were conditioned in a climate chamber at 65% relative humidity and 20°C prior to testing.

The small-scale specimen testing was conducted according to the international standard ISO 13061-6 [37]. The specimen dimensions, however, deviate from the standard (see Sect. 2.1). Density ρ was determined, according to the mass and volume, from the gauge portion, directly after testing. Specimen experiencing a loss of material from the gauge region during testing ($n = 11$) were excluded from ρ analysis.

Testing of the 3500 mm long timber boards was performed according to the European standard EN 408 [38]. The testing machine grip length was 370 mm and the test length (distance between the grips) was 2760 mm. The mean ρ of the timber boards was determined prior to testing.

2.6 Visual inspection and scribe angle measurement

Prior to the tensile tests, all specimens were inspected for visual growth characteristics. On both the timber boards and small-scale specimens, the presence and location of flame wood was recorded. An example of flame wood on a timber board is shown in Fig. 2.

On the timber boards, the position and size of all knots ($\emptyset \geq 10$ mm) were measured by hand. Additionally, the presence of pith and other visual characteristics, such as bark inclusions and discolourations, were recorded.

After testing, visual inspection of the fractured surfaces was made in order to classify the various failure types. In line with other studies [19, 22], the true fibre direction may be revealed from a fractured specimen. Accordingly, a mean fracture angle β of the small-scale specimens was manually determined from the failed specimens. Each surface of a specimen, observed to have a fracture representative of the actual fibre direction (i.e. a fracture path that follows the

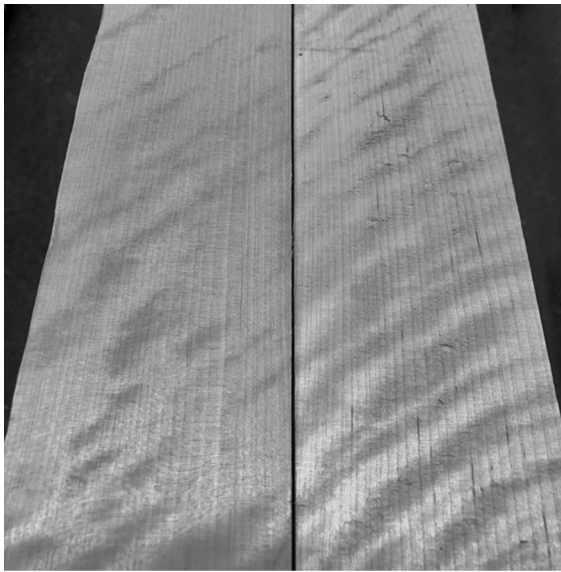


Fig. 2 Examples of flame wood on the tangential surface of timber boards

grain direction), was identified. For all identified surfaces, the representative fracture path was determined using close-up images of the fracture and visually fitting a line to the average fibre direction. β was calculated as the angle between the representative fracture path and the longitudinal direction of the specimen. The fracture angle serves as a reference for evaluation of the detected laser angles.

For the timber boards, the global grain angle is considered. For the purpose of investigating the effect of global grain angle on strength, a classification system is used to separate grain angle related failures from other failures. Grain angle related failures are those dominated by obvious global slope of grain, free from local grain deviations or with apparently insignificant local grain deviations. In addition, knot classified failures are characterised by dominant local grain deviations around knots or from apparent nearby knots outside the timber board; grip failures involve the tensile testing device grips; and failures with other unclear or less common strength reducing features are classified as other.

No fracture angle was measured on the timber boards due to the diverse nature of the fractures. Instead, a scribe angle γ was determined on the narrow faces at the fracture region using a scribing tool. The slope of grain was resolved in accordance with the European standard EN 1310 [21]. The mean value of γ

is calculated from the mean slope of grain, i.e the average direction of the scratched lines.

3 Results and discussion for small-scale specimens

On 115 small-scale specimens non-destructive investigations and afterwards tensile tests were performed. The results are summarized in Table 1.

3.1 Laser angle evaluation

The determined laser angles were compared with the fracture pattern of the small-scale specimens in order to evaluate the relationship between fracture angle and surface measured laser angle. A large portion of small-scale specimens fractured in shearing planes along the grain direction, providing a clear, representative measurement for β . In total, β was determined on 143 sides, from 87 different specimens. The results are illustrated in Fig. 3. It is shown that the determined laser angles are well matched with the tensile fracture angles.

A slight bias is also observed between the measurements. On average, the fracture angle is about one degree larger than the laser angle. The bias may be explained by two factors. First, the fractures are often not pure shear failures along the grain direction but also include some minor (tensile) fracturing across the grain, whereby making the fracture angle larger than the laser angle. Second, as the distance between laser points is relatively large, if the fracture is curved, the location of the laser point within the fracture region may be positioned only at shallower grain angles. This

Table 1 Summary of the test results on small-scale specimens

| Property | | <i>n</i> | Mean value | COV |
|------------------------------|----------------------|----------|------------|------|
| Laser angles (°) | $\alpha_{3D,mean}$ | 115 | 6.3 | 0.57 |
| | $\alpha_{3D,mean}^f$ | 115 | 6.9 | 0.58 |
| | α_{mean}^f | 143 | 5.4 | 0.77 |
| Fracture angle (°) | β | 143 | 6.4 | 0.71 |
| Tensile strength (MPa) | f_t | 115 | 78.0 | 0.38 |
| Density (kg/m ³) | ρ | 104 | 630 | 0.07 |

COV: coefficient of variation

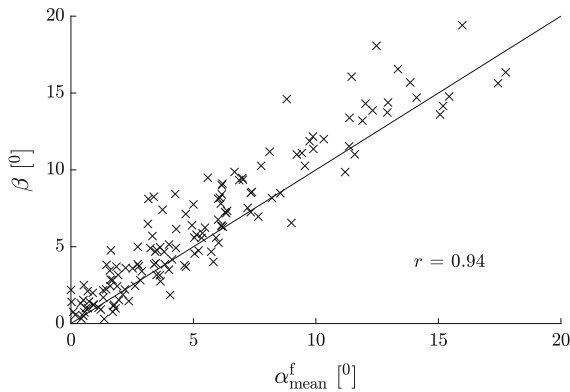


Fig. 3 Comparison between the fracture angle β and the laser angle α_{mean}^f for small-scale specimens

is a form of instrumental error that could be reduced with an increase in laser point density.

In a recent study [22], the grain angle estimated from laser imaging was compared to a splitting angle determined from an automatic splitting device. The correlation obtained for silver birch knot-free specimens, in that study, was lower than the one obtained in the present study. However, it was reported that the splitting method applied for the reference angle contained sources of error and the elliptical recognition algorithms were not specifically optimized for birch [22].

3.2 The influence of laser angle on tensile strength

The relationship between $\alpha_{3D,\text{mean}}^f$ and f_t is shown in Fig. 4. A non-linear dependency is apparent. Failure criteria curves according to Hankinson's formula [40] and a multi-surface failure criteria (MSFC) defined in [39] underlie the data in Fig. 4. The general fit between the observed data and the failure criteria curves indicates suitable approaches for describing the relationship between strength and laser angle measurements. The material properties applied in the failure criteria are obtained from [41, 42]; where tensions strength parallel to the grain, perpendicular to grain, and shear strength are $f_{t,0} = 119$ MPa, $f_{t,90} = 7.16$ MPa, and $f_v = 9.8$ MPa, respectively. Transverse isotropy of the material is assumed.

The exponential parameter for Hankinson's formula is fit to the data by method of least squares, resulting in a value of $n = 1.56$. This exponent is within the range (1.5 to 2.0) regarded suitable for

predicting the (off-axis) tensile strength of wood [18]. In the MSFC, two criteria are applied: a maximum stress criterion for tensile stress parallel to the grain σ_0 , according to Eq. 2, and a quadratic criterion which considers the interaction of tension stress perpendicular to the grain σ_{90} and (longitudinal) shear stress τ , according to Eq. 3. The MSFC curve shown in Fig. 4 is the governing case of the two criteria.

$$\frac{\sigma_0}{f_{t,0}} \leq 1 \quad (2)$$

$$\left(\frac{\sigma_{90}}{f_{t,90}}\right)^2 + \left(\frac{\tau}{f_v}\right)^2 \leq 1 \quad (3)$$

The specimens were classified according to the fracture pattern. Failure classifications, their descriptions, and a summary of the results are given in Table 2. The failure classification is also indicated for each specimen in Fig. 4.

The individual failure modes are partially described by the MSFC. Specimens classified as sloping shear type failures are described by the criterion of Eq. 3, in particular at higher angles. At lower angles, where the longitudinal tensile strength is assumed to govern (Eq. 2), mainly tension, splintering, and longitudinal shear failures are found.

It is important to note that the gauge length of the specimens (200 mm) allowed sloping shear failures greater than 4° to freely occur. Failure predominately took place in the gauged region. However, in 14 specimens, the fracture extends outside the gauge length and these specimens are for the most part, assigned to splintering/longitudinal shear type failures. They are included in the results as their influence on overall sample statistics are assumed to be insignificant, but it is mentioned that the f_t of these specimens may have been affected. This feature of the test setup may explain why sloping shear failures are not observed at $\alpha_{3D,\text{mean}}^f < 4^\circ$ and splintering/longitudinal shear failures are largely at $\alpha_{3D,\text{mean}}^f < 4^\circ$.

In this analysis, the paired specimens, i.e. two adjacent specimens derived from the same timber board, are considered as two independent data. However, if the mean grain angle and mean tension strength of the pairs is considered instead, the results would be similar.



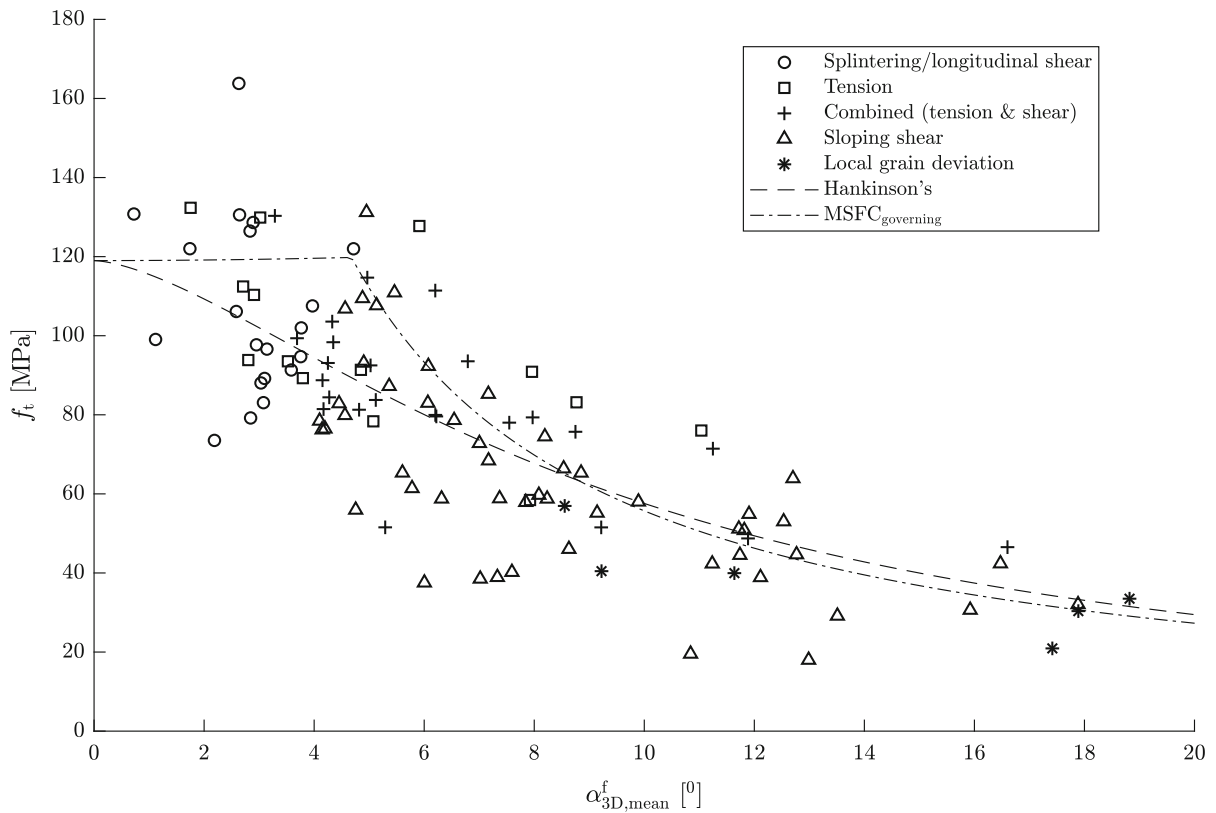


Fig. 4 Dependency between tension strength f_t and laser angle $\alpha_{3D,mean}^f$ for small-scale specimens. Failure classification is detailed for each specimen. Failure criteria: generalized

Hankinson's equation and a multi-surface failure criterion (MSFC) according to [39] is underlain

Table 2 Failure classification of small-scale specimens

| Type of failure | Characteristics | Number of specimens | Mean value | |
|--------------------------------|----------------------------------------------------|---------------------|--------------------------|-------------|
| | | | $\alpha_{3D,mean}^f$ [°] | f_t (MPa) |
| Splintering/longitudinal shear | Fractures along the grain | 20 | 2.9 | 106.6 |
| Tension | Fractures across the grain | 14 | 5.1 | 97.7 |
| Combined | Mixed fractures (usually tension & shear) | 24 | 6.5 | 84.1 |
| Sloping shear | Fractures along the sloped grain | 51 | 8.4 | 63.4 |
| Local grain deviation | Fractures along (curved) localized grain deviation | 6 | 13.9 | 37.0 |

3.3 Flame wood

In general, the fracture of flame wood specimens follow, to a certain extent, the wavy grain direction. The wavy nature of the flame wood regions are identified in the laser angles and appear as large local fluctuations. Although a higher density of laser points

may provide a better reading of the wave-like properties, as the wavy grains were sometimes localized to a few centimetres or less, the location and intensity of the flame wood is reflected in the laser angle data.

Specimen with flame wood are also concerned with larger grain angles $\alpha_{3D,mean}$, compared to non-flame wood specimens, Fig. 5(left). Flame wood also has an

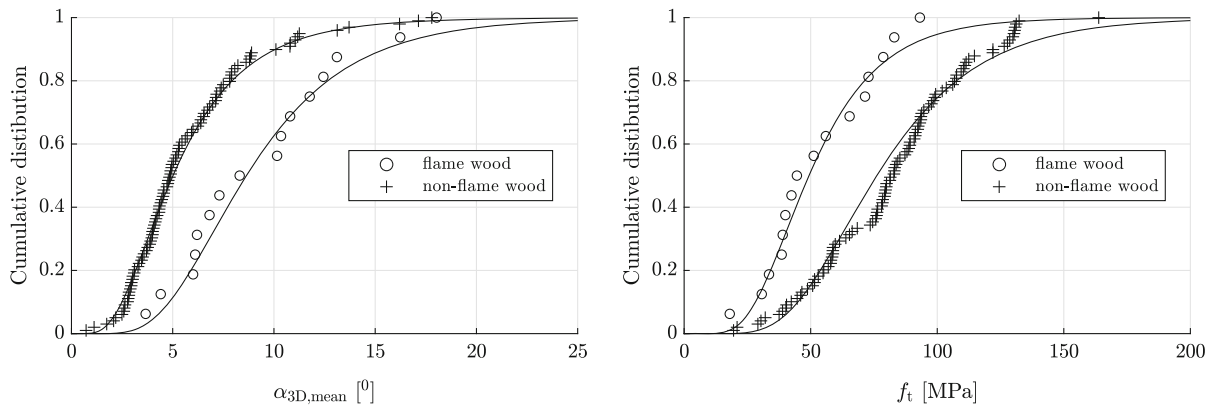


Fig. 5 Cumulative distribution of tension strength f_t and laser angle $\alpha_{3D,mean}$ for small-scale specimens with and without flame wood. The empirical data is fit with a log-normal distribution (solid lines)

apparent influence on strength as the distribution of f_t of specimens with flame wood is clearly shifted towards lower strength values, Fig. 5(right). For both $\alpha_{3D,mean}$ and f_t , independent samples t -tests indicate statistically significant (p values < 0.001) differences between the flame wood and non-flame wood samples. These result are further expressed in the correlation between f_t and $\alpha_{3D,mean}$ for flame wood specimens with $r = -0.79$.

The ρ of specimens with flame wood is, in general, higher than specimens without (Fig. 6). The mean value of ρ for flame wood and non-flame wood specimens is 675 kg/m^3 and 624 kg/m^3 , respectively. Independent samples t -test further suggest statistical significance in the difference (p value < 0.001).

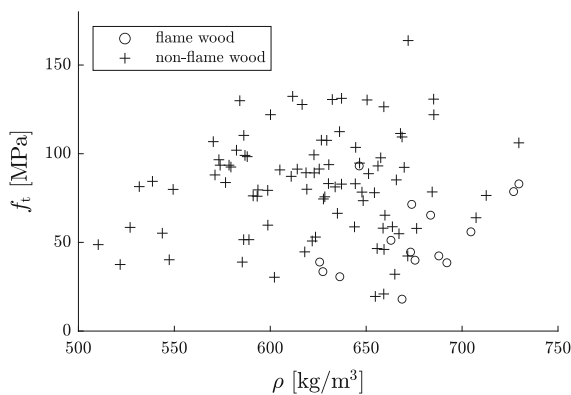


Fig. 6 Comparison between tension strength f_t and density ρ for small-scale specimens

While information on the physical and mechanical properties of flamy-grained birch is lacking in the literature, curly-grained birch, another variation of silver birch with abnormal growth patterns, has received some attention. Like the results observed in the present study, curly-grained birch has also exhibited higher density and lower tensile strengths compared with normal silver birch wood [31].

3.4 Density

Density does not have an unambiguous influence on strength ($r(f_t, \rho) \approx 0$) for this sample (Fig. 6). This is partially due to the dominant influence of grain angle. When specimens with low grain angles are exclusively considered, a slight correlation can be observed, e.g. for $\alpha_{3D,mean} < 6^\circ$ the correlation is $r = 0.23$. This still minor relationship suggest that ρ has only a slight influence on the tension strength of birch. A similar result is reported for yellow birch [16]. As noted by [43] the ultra-structure (characteristics at the cellular level) may be more influential than density for tension strength parallel to the grain.

4 Results and discussion for timber boards

On 70 timber boards, non-destructive investigations and tensile tests were performed. Global grain angle was a major influencing factor leading to a significant number of failures ($n = 24$). Laser angles were measured on the two narrow faces and a median value of the laser angles (from the more severe side of the

board) in the fracture region, α_{median}^f , is considered for analysis. The median value is selected as it is less sensitive to local disturbances and outlier measurements. The measurement results are summarized in Table 3. Laser and scribe angles are reported only for boards with global grain angle related failures.

4.1 Laser angle and timber board strength

Timber board failure modes were classified according to visual inspections of the fracture and the apparent strength determining characteristic. Timber boards with grain angle related failure are mainly of interest for comparisons with α_{median}^f . In Fig. 7, failures related to grain angle are shown along with failures related to knots and knot clusters, grips and other defects. When only timber boards with grain angle related failures are considered, the correlation between α_{median}^f and f_t is $r = -0.58$. This relationship indicates that the laser determined global grain angle is relevant for the tensile strength of timber boards. It is noted that for the prediction of strength, it is essential to consider the effect of knots. The measurement of local grain deviations through full board scanning could allow also knot related grain deviations to be measured, and strength predictions for all timber boards, e.g. [25, 44].

The observed relationships also show that narrow face scanning may be an applicable method to non-destructively evaluate existing structures in which only the narrow faces of timber lamella are visible, e.g. in glued laminated timber elements.

Because laser imaging of the timber boards was conducted after tension testing, in two cases, boards with grain angle related failures had material loss (on the narrow faces, at fracture) that resulted in non-acceptance of laser points. In these cases, the neighbouring areas were considered representative.

Table 3 Summary of the test results on timber boards

| Property | | <i>n</i> | Mean value | COV |
|------------------------------|----------------------------|----------|------------|------|
| Laser angles (°) | α_{median}^f | 24 | 6.9 | 0.51 |
| Scribe angle (°) | γ_{mean}^f | 24 | 6.5 | 0.31 |
| Tension strength (MPa) | f_t | 70 | 43.5 | 0.29 |
| Density (kg/m ³) | ρ | 70 | 653 | 0.07 |

COV: coefficient of variation

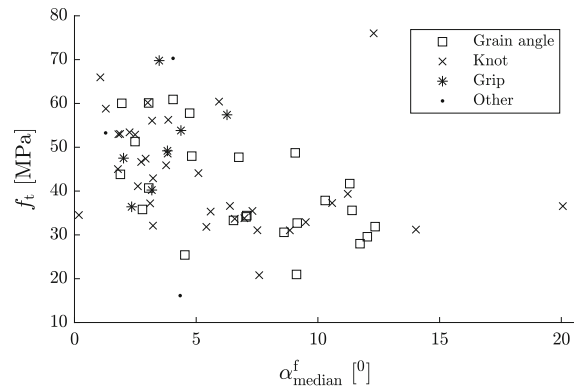


Fig. 7 Comparison between tension strength f_t and the laser angle α_{median}^f for timber boards

4.2 Scribing method

The results from the laser measurement were compared with those from the scribing tool. The scribe angles provide a measure of the grain angle (on the surface) within the fracture region. In comparing the methods, the relationship between γ_{mean}^f and α_{median}^f , $r = 0.71$, indicates a good agreement. While this result further indicates that the laser angles appropriately estimate the actual fibre direction, it is noted that the scribing method, as a semi-destructive contact method, can be involved with user error.

4.3 Flame wood

The appearance of flame wood was observed during the visual inspection. As mentioned, in this study, the position of each individual timber board within the tree stem was known [33]. Therefore, the presence of flame wood within the tree can be described. For the most part, flame wood was found on the lower ends of the timber boards, i.e. the lower portion of the tree, and more concentrated at regions furthest from the pith.

Although the laser resolution on the timber boards was rather sparse, the wave like variations could be detected in most cases where the flame wood was visually observed on the narrow faces.

Figure 8 shows the cumulative distributions of f_t for specimens with and without flame wood. Contrary to results observed on the small-scale specimen, flame wood does not have an apparent influence on f_t of timber boards. In terms of an independent samples *t*-

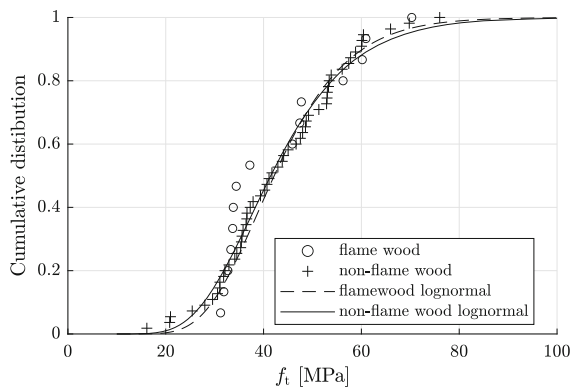


Fig. 8 Distribution of tension strength f_t for timber boards with and without flame wood

test, the difference between the tension strength of timber boards with and without flame wood was not statistically significant (p value = 0.46). The reason for this may be due to the localized presence on the boards as it may occur only within some annual rings and not over the full cross section. Furthermore, other features such as spiral grain, diagonal grain, and knots may be associated with more severe strength reductions. Visual inspection of the fracture of timber boards failing in regions with flame wood reveals that the fracture does tend to follow the wavy grain direction, although, larger less-localized deviations are also commonly present.

In terms of density, it is found that timber boards with flame wood have a similar (mean) ρ as boards without flame wood.

4.4 Relationships between timber boards and small-scale specimens

The relationship between f_t of small-scale specimen and timber boards is shown in Fig. 9. No unambiguous correlation is observed when all specimens are considered. This is not surprising as the knots and other localized defects have a major influence on the f_t of timber boards. When timber boards with grain angle related failures are exclusively considered, the correlation is $r = 0.51$. This dependency may be related to global grain angle characteristics, e.g. spiral grain, identified at both scales.

In this analysis, the paired specimens, i.e. two adjacent specimens derived from the same timber board, are considered as two independent data.

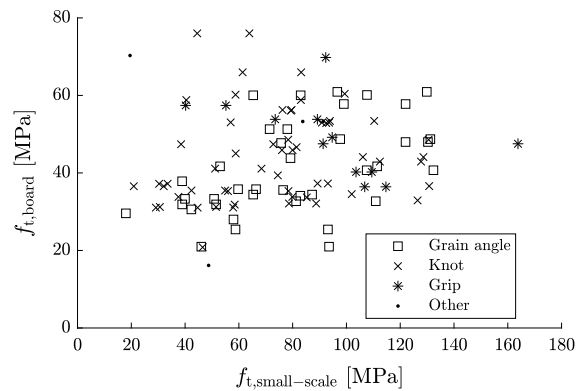


Fig. 9 Comparison of tension strengths f_t for small-scale specimens and timber boards, along with the corresponding failure mode of the timber boards

However, if the mean f_t of the pairs is considered instead, the results would be similar.

In further analysis of the paired specimens, the difference in $\alpha_{3D,mean}$ and f_t between the pairs is investigated. It is observed that the mean and maximum difference in f_t was 21 MPa and 72 MPa, respectively; and the mean and maximum difference in $\alpha_{3D,mean}$ was 2.1° and 11.4° , respectively. Considering that the pairs are cut from adjacent positions these difference are rather high. This reflects the highly localized material properties.

5 Conclusion and outlook

The present paper investigates a laser light scattering technique for the non-destructive measurement of grain angle on silver birch. The method was evaluated on small-scale and large-scale (timber board) specimens, which are destructively tested under tension loading.

The laser determined grain angles compared well with observed tensile fracture angles of the small-scale specimens (correlation coefficient $r = 0.94$). Three-dimensional laser angles, derived from surface measurements on all four sides of the small-scale specimens, show a clear relationship with tension strength, and can be described with failure criteria from the literature. Laser angles, determined on the narrow faces of the timber boards, indicate that the method is suitable for the measurement of global grain angles. The global grain angles are found relevant for tension strength, however, higher measurement resolution was

needed for the quantification of more severe localized grain deviations around strength reducing defects.

Laser scattering in regions with flame wood, a genetic modification of silver birch associated with wave-like grain deviations, showed that grain angle related characteristics of this wood type can be identified. It was found that small-scale specimens with flame wood tend to have higher grain angles and lower strength, relative to specimens without. For timber boards, fluctuations in grain angles were observed in flame wood regions, however, no unambiguous influence of flame wood on the strength was identified.

The results presented in this paper indicate laser scattering to be an applicable method for grain angle determination on silver birch, and therefore, indicate the potential for strength predictions. Future research should extend the method for the purpose of strength predictions of birch timber boards, whereby, full-board laser scanning is proposed for the measurement of both global and local grain deviations.

Acknowledgements The authors acknowledge B.Sc. Henri Ranttila for his invaluable contribution to the experimental investigations.

Funding Open Access funding provided by Aalto University.

Declarations

Conflict of interest The authors declare that they have no conflict of interest.

Open Access This article is licensed under a Creative Commons Attribution 4.0 International License, which permits use, sharing, adaptation, distribution and reproduction in any medium or format, as long as you give appropriate credit to the original author(s) and the source, provide a link to the Creative Commons licence, and indicate if changes were made. The images or other third party material in this article are included in the article's Creative Commons licence, unless indicated otherwise in a credit line to the material. If material is not included in the article's Creative Commons licence and your intended use is not permitted by statutory regulation or exceeds the permitted use, you will need to obtain permission directly from the copyright holder. To view a copy of this licence, visit <http://creativecommons.org/licenses/by/4.0/>.

References

- Isaksson T (1999) Modelling the variability of bending strength in structural timber-length and load configuration effects. Ph.d. thesis, Dissertation, Lund University
- Fink G, Kohler J (2014) Model for the prediction of the tensile strength and tensile stiffness of knot clusters within structural timber. *Eur J Wood Wood Prod*. 72:331–341
- Sandberg D, Fink G, Hasener J, Kairi M, Ross RJ, Steiger R, Marhenke T, Wang X (2022) Process control and grading in primary wood processing. In: Peter N, Alfred T, Dick S (eds) Springer handbook of wood science and technology. Springer, Berlin
- EN 384 (2016) Structural timber. Strength classes. European Committee for Standardization, Brussels
- Solli KH (2004) Tensile strength of Nordic birch. In: Proceedings of meeting thirty-seven of CIB-W18, paper 37-6, 1
- van de Kuilen JW, Blaß HJ (2005) Mechanical properties of azobé (*lophira alata*). *Holz als Roh-und Werkstoff* 63:1–10
- Frühwald K, Schickhofer G (2005) Strength grading of hardwoods. In: Proceedings of the 14th international symposium on nondestructive testing of wood, vol 2
- Kilde V, Solli KH, Pitzner B, Lind P, Bramming J (2006) Bjørk i synlige konstruksjoner (Birch in visible constructions). Technical Report Rapport nr. 67, Norsk Treteknisk Institutt
- Ehrhart T, Fink G, Steiger R, Frangi A (2016) Strength grading of European beech timber for the production of GLT & CLT. In: International network on timber engineering research: proceedings of meeting 49. 49, pp 29–44. <https://doi.org/10.3929/ethz-a-010795316>
- Jeitler G, Augustin M, Schickhofer G (2016) Birch glt+ clt-mechanical properties of glued laminated timber and cross laminated timber produced with the wood species birch. In: Proceedings of world conference on timber engineering, Wien, Austria, pp MS1–07
- Weidenhiller A, Linsenmann P, Lux C, Brüchert F (2019) Potential of microwave scanning for determining density and tension strength of four European hardwood species. *Eur J Wood Wood Prod* 77:235–247. <https://doi.org/10.1007/s00107-019-01387-x>
- Kovryga A, Stapel P, van de Kuilen JW (2020) Mechanical properties and their interrelationships for medium-density European hardwoods, focusing on ash and beech. *Wood Mater Sci Eng* 15(5):289–302. <https://doi.org/10.1080/17480272.2019.1596158>
- Brunetti M, Nocetti M, Pizzo B, Aminti G, Cremonini C, Negro F, Zanuttini R, Romagnoli M, Mugnozza GS (2020) Structural products made of beech wood: quality assessment of the raw material. *Eur J Wood Wood Prod* 78:961–970. <https://doi.org/10.1007/s00107-020-01542-9>
- Kovryga A, Sarnaghi AK, van de Kuilen JW (2020) Strength grading of hardwoods using transversal ultrasound. *Eur J Wood Wood Prod* 78:951–960. <https://doi.org/10.1007/s00107-020-01573-2>
- Ravenshorst G, Gard W, van de Kuilen JW (2020) Influence of slope of grain on the mechanical properties of tropical hardwoods and the consequences for grading. *Eur J Wood Wood Prod* 78:915–921. <https://doi.org/10.1007/s00107-020-01575-0>
- Morin-Bernard A, Blanchet P, Dagenais C, Achim A (2020) Strength grading of northern hardwood species for structural engineered wood products: identification of the relevant indicating properties. *BioResources* 15(4):8813–8832. <https://doi.org/10.15376/biores.15.4.8813-8832>



17. Luostarinen K, Verkasalo E (2000) Birch as sawn timber and in mechanical further processing in Finland. A literature study. *Silva Fennica Monogr* 1:40
18. Kollmann FF, Côté WA Jr (1968) Principles of wood science and technology, vol I. Solid Wood. Springer, New York
19. Ehrhart T, Steiger R, Frangi A (2018) A non-contact method for the determination of fibre direction of European beech wood (*Fagus sylvatica* L.). *Eur J Wood Wood Prod* 76:925–935. <https://doi.org/10.1007/s00107-017-1279-3>
20. Collins S, Fink G (2022) Modeling the tensile mechanical properties of silver birch timber boards. *Construct Build Mater*. <https://doi.org/10.1016/j.conbuildmat.2022.128147>
21. EN 1310 (1997) Round and sawn timber. method of measurement of features. European Committee for Standardization, Brussels
22. Schlotzhauer P, Wilhelms F, Lux C, Bollmus S (2018) Comparison of three systems for automatic grain angle determination on European hardwood for construction use. *Eur J Wood Wood Prod* 76:911–923. <https://doi.org/10.1007/s00107-018-1286-z>
23. Shen J, Zhou J, Vazquez O (2000) Experimental study of optical scattering and fiber orientation determination of softwood and hardwood with different surface finishes. *Appl Spectrosc* 54(12):1793–1804
24. Zhou J, Shen J (2003) Ellipse detection and phase demodulation for wood grain orientation measurement based on the tracheid effect. *Opt Lasers Eng* 39(1):73–89
25. Rais A, Bacher M, Khaloian-Sarnaghi A, Zeilhofer M, Kovryga A, Fontanini F, Hilmers T, Westermayr M, Jacobs M, Pretzsch H, van de Kuilen JW (2021) Local 3d fibre orientation for tensile strength prediction of European beech timber. *Constr Build Mater*. <https://doi.org/10.1016/j.conbuildmat.2021.122527>
26. Olsson A, Pot G, Viguier J, Faydi Y, Oscarsson J (2018) Performance of strength grading methods based on fibre orientation and axial resonance frequency applied to norway spruce (*Picea abies* L.), douglas fir (*Pseudotsuga menziesii* (mirb.) franco) and European oak (*Quercus petraea* (matt.) Liebl./*quercus robur* L.). *Ann For Sci* 75(4):1–18
27. Hu C, Tanaka C, Ohtani T (2004) On-line determination of the grain angle using ellipse analysis of the laser light scattering pattern image. *J Wood Sci* 50(4):321–326
28. Besseau B, Pot G, Collet R, Viguier J (2020) Influence of wood anatomy on fiber orientation measurement obtained by laser scanning on five European species. *J Wood Sci* 66(1):1–12
29. Simonaho SP, Palviainen J, Tolonen Y, Silvennoinen R (2004) Determination of wood grain direction from laser light scattering pattern. *Opt Lasers Eng* 41:95–103. [https://doi.org/10.1016/S0143-8166\(02\)00144-6](https://doi.org/10.1016/S0143-8166(02)00144-6)
30. Verkasalo E, Heräjärvi H, Möttönen V, Haapala A, Brännström H, Vanhanen H, Miina J (2017) Current and future products as the basis for value chains of birch in finland. In: Proceedings of the International Scientific Conference on Hardwood Processing, Lahti, Finland
31. Hintikka T (2004) Visakoivun lujuusominaisuuksien selvittäminen kokeellisesti. Turun ammattikorkeakoulu (in Finnish)
32. Viherä-Aarnio A, Hagqvist R (2017) Curly birch (*Betula pendula* var. *carelica*), wooden “marble” from finland-soon easily available. In: Proceedings of the international scientific conference on hardwood processing, Lahti, Finland
33. Collins S, Fink G (2020) Mechanical behaviour of sawn timber of silver birch under compression loading. *Wood Mater Sci Eng*. <https://doi.org/10.1080/17480272.2020.1801836>
34. Collins S, Fink G (2018) Mechanical properties of birch timber under compression loading parallel to the grain. In: Proceedings of World Conference on Timber Engineering, Seoul, Republic of Korea
35. Jiandong H (2010) Ellipse detection based on principal component analysis. In: International conference on computer application and system modeling, vol 9. IEEE, pp V9–258–V9–261. <https://doi.org/10.1109/ICCASM.2010.5623040>
36. Matthews PC, Soest JF (1986) Method for determining localized fiber angle in a three dimensional fibrous material. US Patent 4606645
37. ISO 13061–6:2014(E), (2014) Physical and mechanical properties of wood - test methods for small clear wood specimens - part 6: determination of ultimate tensile stress parallel to grain. International Organization for Standardization, Geneva
38. EN 408 (2012) Timber structures - Structural timber and glued laminated timber - determination of some physical and mechanical properties. European Committee for Standardization, Brussels
39. Sandhaas C, van de Kuilen JWG (2013) Material model for wood. *Heron* 58(2–3):171–91
40. Hankinson R (1921) Investigation of crushing strength of spruce at varying angles of grain. *Air Serv Inform circular* 3(259):130
41. Jalava M (1945) Suomalaisen männyn, kuusen, koivun ja haavan lujuusominaisuuksista. (Strength properties of Finnish pine, spruce, birch and aspen). *Metsätieteellisen Tutkimuslaitoksen Julkaisuja*
42. Pramreiter M, Bodner SC, Keckes J, Stadlmann A, Kumpenza C, Müller U (2020) Influence of fiber deviation on strength of thin birch (*Betula pendula* Roth.) veneers. *Materials* 13: 7. <https://doi.org/10.3390/ma13071484>
43. Dinwoodie JM (2000) Timber: its nature and behaviour. CRC Press, London
44. Briggert A, Olsson A, Oscarsson J (2020) Prediction of tensile strength of sawn timber: definitions and performance of indicating properties based on surface laser scanning and dynamic excitation. *Mater Struct* 53:1–20

Publisher's Note Springer Nature remains neutral with regard to jurisdictional claims in published maps and institutional affiliations.

